electronics

MDPI

Article

A High-Precision Measurement Method for Radar Antenna Scan Period in Complex Filed Environments Suitable for Engineering Implementation

Bin Wang and Min Wang *

Key Laboratory of Specialty Fiber Optics and Optical Access Networks, Shanghai Institute for Advanced Communication and Data Science, Shanghai University, Shanghai 200444, China; wang_bin@shu.edu.cn
* Correspondence: wangmin@mail.shu.edu.cn

Abstract

The antenna scan period is a core technical parameter of radar, and its robust, real-time, and high-precision measurement is of great engineering significance. Based on filed-measured full-pulse radar data, two measurement methods for the antenna scan period are proposed in this paper: the smoothing-fitting method and the smoothing-correlation method. Verified by filed-measured data, the measurement error fluctuation of the smoothing-fitting method is no more than 2 pulse repetition intervals (PRIs), and that of the smoothing-correlation method is no more than 1 PRI, both meeting the requirements of engineering applications. Adopting a point-by-point sliding processing flow without batch fitting, the smoothing-correlation method is more suitable for streaming and real-time data processing compared with the smoothing-fitting method and has a distinct engineering transformation value. Compared with batch processing methods such as the cepstrum method, which need to buffer data of at least one complete scanning period, the smoothing-correlation method avoids full-sequence FFT/IFFT operations. It can significantly reduce memory occupation and processing time and achieve superior real-time performance.

Keywords: radar antenna scan period; pulse description word; filed measurement; smoothing-fitting method; smoothing-correlation method

1. Introduction

The antenna scan period is a core technical parameter of radar, which directly reflects the rotation law and beam scanning characteristics of radar antennas, and serves as a critical basis for radar signal sorting and emitter identification [1,2]. With the increasingly complex electromagnetic environment, the density of radar signals continues to rise and clutter interference becomes more severe, leading to three core limitations of traditional measurement methods for the radar antenna scan period [3]: first, low measurement accuracy—most traditional methods rely on simple pulse amplitude threshold judgment and statistical analysis of the interval between adjacent antenna mainlobe beams, which are susceptible to pulse loss and amplitude jitter [4], making it difficult to meet the demand for high-precision measurement; second, poor anti-interference robustness—such methods exhibit insufficient stability under non-ideal working conditions including outdoor noise, amplitude distortion, and flat peak values [5], which easily causes positioning deviation of the mainlobe beam; third, no support for streaming real-time processing—most methods adopt offline operation with batch data and cannot adapt to the real-time pulse stream processing architecture [6],

Academic Editor: Emanuele Cardillo

Received: 3 April 2026
Revised: 17 May 2026
Accepted: 20 May 2026
Published: 22 May 2026

resulting in great difficulty in engineering implementation. Therefore, developing a radar antenna scan period measurement technology with high measurement accuracy, strong anti-interference ability and easy engineering implementation for filed-measured data is of important practical significance.

In recent years, scholars at home and abroad have carried out extensive research on radar scan period measurement and proposed various improved methods for traditional threshold detection [7,8], curve fitting [9–11], and spectrum estimation [12]. However, most of these methods are verified based on ideal simulation data and have insufficient adaptability to filed-measured data in complex real outdoor environments [13]; some methods have excessively high computational complexity and cannot support streaming real-time processing [14]; others have weak anti-interference ability and poor measurement stability, showing insufficient robustness when facing pulse distortion and amplitude fluctuation caused by the complex outdoor electromagnetic environment [15], which is difficult to meet actual engineering needs. Meanwhile, some existing algorithms mostly rely on offline batch data processing, cannot adapt to the pulse streaming real-time processing architecture, and pose great challenges for engineering implementation.

Combined with the requirements of engineering implementation and based on filed-measured full-pulse data, this paper fully considers the actual conditions such as noise interference, abnormal pulses and limited processing resources, and proposes two high-precision measurement methods: the smoothing-fitting method and the smoothing-correlation method. Noise interference is suppressed through data smoothing preprocessing, and the antenna mainlobe pattern is reconstructed via least square fitting, while the periodic characteristics are extracted through cross-correlation operation, respectively, to achieve accurate calculation of the antenna scan period. The main contributions of this paper are as follows:

1. Based on filed-measured PDW data instead of ideal simulation data, this paper proposes the smoothing-fitting and smoothing-correlation methods to address the problems of noise interference and amplitude distortion in filed-measured data, which effectively improve the stability and accuracy of scan period measurement in complex electromagnetic environments and solve the pain points of low measurement accuracy and insufficient robustness of existing methods in practical outdoor scenarios.
2. The processing flow of the proposed smoothing-correlation method is similar to that of the classic pulse compression algorithm for radar signal processing, which is compatible with the streaming real-time processing architecture, convenient for hardware engineering implementation, and has direct engineering application value for airborne/vehicle-borne radar reconnaissance and real-time radar signal sorting systems.
3. The proposed algorithms are verified based on filed-measured data and compared with the traditional threshold method, curve fitting method and spectrum estimation method. Experimental results show that the smoothing-correlation method achieves the optimal comprehensive performance, with its measurement accuracy significantly leading among the five methods. It is consistent with the existing pulse compression algorithm processing architecture and has high engineering adaptability and low storage overhead. Although it has the largest amount of computation, real-time processing can be realized through optimization methods such as parallel computing on modern processor platforms, making it the preferred solution for high-precision radar antenna scan period measurement scenarios, including radar emitter identification.

This paper first expounds the basic measurement model of radar antennas and the characteristics of filed-measured data, then introduces in detail the principles, implementation flows and calculation steps of the two measurement methods (smoothing-fitting and smoothing-correlation). Subsequently, comparative verification is carried out with filed-measured data to analyze the measurement accuracy, error fluctuation and engineering applicability of the two methods. Finally, the advantages of the methods are summarized to provide an engineering reference for the real-time and high-precision measurement of the radar antenna scan period.

2. Model and Data

2.1. Measurement Model

It is assumed that the radar antenna operates in a mechanical uniform-speed circular scanning mode. The antenna scan period of a mechanically scanned radar is defined as the time interval between two consecutive pointing of the antenna mainlobe beam to the same azimuth, and its mathematical expression can be written as:

$$T = t_{i+1} - t_i \tag{1}$$

where t_{i+1} and t_i represent the corresponding times when the antenna mainlobe beam points to the same azimuth in two adjacent instances, respectively.

Let the pulse repetition interval of the radar be PRI, and the time of arrival (TOA) of the k-th pulse be TOA_k. Then the pulse time sequence satisfies:

$$TOA_k = TOA_1 + (k-1)PRI + \varepsilon_k \tag{2}$$

where ε_k is the measurement noise and time jitter.

The core task of radar antenna scan period measurement is to accurately extract the time difference between two adjacent instances when the antenna mainlobe beam is aligned with the same azimuth from the intercepted pulse sequence, so as to complete the estimation of the antenna scan period.

It should be specifically noted that the radar antenna scanning period is a slow-period feature determined by the mechanical rotation of the antenna, reflecting the time required for the antenna beam to complete one full scan, and belongs to macro envelope modulation. In contrast, the pulse repetition interval (PRI) is a fast period generated by the internal timing of the radar, belonging to micro pulse timing. The scanning period is extracted by accurately capturing the time difference between two consecutive instances when the antenna mainlobe beam points to the same azimuth, relying on the pulse amplitude envelope characteristics. This method is independent of the timing law of the time of arrival (TOA) of pulses, and thus is not affected by the fixed, jittering, staggered, or sliding variations in PRI. Even under non-constant timing conditions, the measurement model remains stable.

2.2. Filed Measured Data

The data used in this paper are obtained from the actual interception of a mechanically scanned radar in an outdoor environment, and the research is carried out based on the sorted radar Pulse Description Word (PDW) dataset. The PDW includes Time of Arrival (TOA), Pulse Amplitude (PA), Radio Frequency (RF), Pulse Width (PW) and Direction of Arrival (DOA). The k-th PDW is recorded as:

$$PDW_k = [TOA_k, PA_k, RF_k, PW_k, DOA_k] \tag{3}$$

This dataset contains 10,000 effective pulses with a signal duration of approximately 36.5 s, and the nominal value of the radar antenna scan period is 10 s. The data length covers 3 complete scan periods, which can meet the requirements of high-precision measurement of the antenna scan period. The calculated pulse repetition interval is about 3.65 ms (fixed PRI), with approximately 2740 pulses and 120 mainlobe pulses in one scan period.

The field measured data was collected in a complex propagation environment in the suburban area of an urban region. Affected by the reflection of buildings, the received signal suffers from obvious multipath propagation interference; meanwhile, it is superimposed with adjacent-frequency civil mobile communication signals. Due to the superposition of multipath interference and electromagnetic interference, the intercepted pulse amplitude sequence exhibits typical phenomena such as random fluctuations and pulse loss. The measured time-series distribution of the radar full-pulse amplitude is shown in Figure 1, and the time-series characteristics of the pulse amplitude within the mainlobe beam are shown in Figure 2.

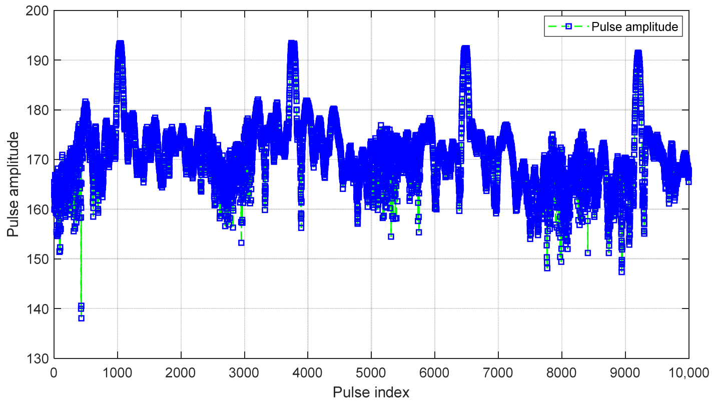

Figure 1. Pulse amplitude-time sequence intercepted in the filed.

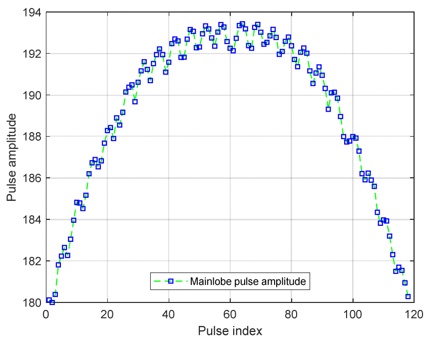

Figure 2. Time-series characteristics of pulse amplitude in the radar mainlobe beam.

2.3. Analysis of Measurement Model

In the actual filed environment, affected by various non-ideal factors such as slight movement of the radar platform (static platform) or even motion (airborne platform), signal propagation attenuation, complex electromagnetic interference and equipment measurement errors, the amplitude of pulses intercepted in the mainlobe beam exhibits significant fluctuations, and the peak value of the pulse amplitude can hardly correspond to the antenna mainlobe vertex accurately. In extreme working conditions, the pulse amplitude in the mainlobe area also exhibits distortions such as amplitude depression and waveform splitting, as shown in Figure 3a. In addition, affected by the width of the radar mainlobe beam, the pulse amplitude near the mainlobe vertex changes gently without obvious peak characteristics, as shown in Figure 3b.

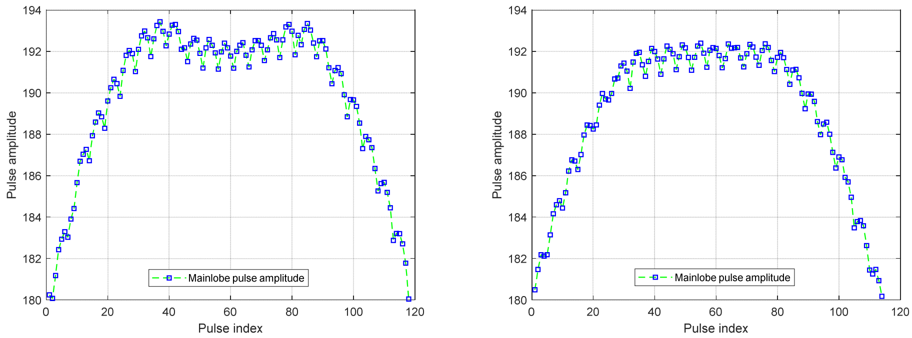

Figure 3. Schematic diagrams of amplitude depression distortion and flat amplitude characteristics of mainlobe pulses: (**a**) Amplitude depression distortion; (**b**) Flat amplitude characteristics.

In the filed environment, the amplitude of the intercepted pulse can be modeled as:

$$PA_k = G(\theta_k) \cdot A_0 + n_k \tag{4}$$

where

$G(\theta_k)$: is the gain of the typical antenna pattern of the radar at the azimuth angle θ_k;

A_0: is the nominal value of the radar transmission amplitude;

n_k: is the channel noise and propagation attenuation, satisfying $n_k \sim N\left(0, \sigma^2\right)$.

The traditional threshold method directly takes $t_i = argmax(PA_k)$, which will cause large measurement errors in the case of pulse amplitude depression and flat peak values.

All the above non-ideal conditions make the traditional method—taking the arrival time of the pulse with the maximum amplitude in the mainlobe pulse group as the reference time—unable to deal with special working conditions such as amplitude depression and flat amplitude, and unable to locate the mainlobe vertex accurately, thus making it difficult to achieve high-precision measurement of the antenna scan period. Aiming at this difficulty, based on the inherent characteristics of filed-measured PDW data, this paper takes the high-precision estimation of the mainlobe vertex as the core goal and proposes two measurement methods adapted to the complex outdoor environment to realize the robust estimation of the radar antenna scan period. Taking the fixed PRI as an example, under the constraint of the actual measured pulse sampling rate (pulse repetition frequency), the scanning period can only be calculated by the number of pulses between adjacent mainlobe vertices. Let the pulse index of the i-th vertex be Ni and the pulse index of the (i + 1)-th vertex be N_{i+1}; the scanning period is expressed as $T = (N_{i+1} - N_i) \times PRI$. Since the vertex can only fall at the moment of a certain pulse rather than between two pulses, the theoretical limit of the measurement accuracy is one PRI.

3. Measurement Methods

Combined with the characteristics of radar PDW data intercepted in the filed environment and aiming at the defects of traditional measurement methods, two high-precision antenna scan period measurement methods are proposed in this paper: the smoothing-fitting method and the smoothing-correlation method. Both methods first suppress noise interference through data smoothing and then complete the mainlobe vertex positioning and period calculation by virtue of curve fitting and cross-correlation operation, respectively. They are adapted to the complex interference environment outdoors and take both measurement accuracy and operation efficiency into account.

3.1. Smoothing-Fitting Method

In practical engineering applications, the Mainlobe Pattern (MBP) of the radar antenna is hidden in the fluctuation of pulse amplitude, and it is usually difficult to obtain its accurate mathematical analytical expression directly, so it is necessary to realize approximate reconstruction by means of data fitting. The core goal of fitting is to construct an explicit function to accurately approximate the pulse amplitude sequence in the measurement period and restore the real beam shape.

The least square fitting method has the advantages of high fitting accuracy, low computational complexity and easy engineering implementation, which is suitable for the processing of filed-measured data. Therefore, this paper adopts this method to reconstruct the MBP curve. Before fitting, it is necessary to perform smoothing preprocessing on the original data. The smoothing processing usually adopts the moving average algorithm, which suppresses noise interference through local averaging, weakens the deviation caused by pulse jitter and abnormal amplitude, and improves the stability and accuracy of subsequent fitting. For the original pulse amplitude sequence $\mathrm{PA} = [PA_1, PA_2, \cdots PA_N]$, the moving average is performed with the window length L, and the smoothed amplitude $\widetilde{\mathrm{PA}}_i$ is:

$$\widetilde{\mathrm{PA}}_i = \frac{1}{L} \sum_{j=i-\frac{L}{2}}^{j=i+\frac{L}{2}} PA_j, (L \le i \le N - L) \tag{5}$$

The noise variance after smoothing satisfies $\sigma^2_{\tilde{n}} = \sigma^2_n / L$; the larger the window, the stronger the noise suppression effect.

Taking data smoothing as the preprocessing step, the smoothing-fitting method reconstructs the antenna mainlobe beam curve combined with least square fitting, obtains the accurate reference time by locating the vertex of the fitting curve, and finally calculates the antenna scan period. The specific implementation steps are as follows:

Step 1: According to the noise jitter level of the original pulse amplitude, the moving average window length L is adaptively selected, combined with the field noise intensity and the radar mainlobe beamwidth. The selection of window length L must simultaneously satisfy three constraint conditions:

First, the mainlobe presents a unimodal and smooth convex envelope curve. To avoid distorting the mainlobe envelope, L should be less than half of the pulse number Nmain within the mainlobe. Excessively large L will overly smooth the mainlobe, causing vertex offset and degradation of estimation accuracy.

Second, to suppress noise effectively, the smoothing window length L needs to cover multiple pulses. The noise suppression capability of smoothing processing is positively correlated with L; a larger L achieves better noise filtering performance.

Third, considering engineering real-time performance, L should be as small as possible. A smaller L leads to lower processing latency.

Therefore, L must be selected as a trade-off among mainlobe envelope integrity, noise suppression performance, and real-time latency. The general engineering selection criterion is L = $\lfloor 1/4N_{main} \rfloor \sim \lfloor 1/3N_{main} \rfloor$, which can balance mainlobe envelope integrity, high-frequency noise suppression, and low-latency requirements.

In the field measured data of this paper, the total number of pulses within a single mainlobe is approximately 120. To quantitatively analyze the influence of smoothing window length L, three typical window lengths L = 10, 20, 30 are set for comparative experiments. The results show that L = 30 can effectively filter random noise and abrupt interference, while completely retaining key features such as the mainlobe rising edge and peak neighborhood. The estimation error of the vertex moment is controlled within 1%, and the low-latency requirement is also satisfied. Consequently, L = 30 is finally determined as the optimal smoothing window length.

Step 2: According to the characteristics of the smoothed pulse amplitude, M sets of complete mainlobe pulse sequence sets are identified and segmented. Taking the m-th group of mainlobe pulses as an example, this group contains N_p pulses, and its pulse amplitude sequence and corresponding time sequence can be expressed as:

$$\widetilde{PA} = \left[\widetilde{\mathrm{PA}_1}, \widetilde{\mathrm{PA}_2}, \cdots, \widetilde{PA}_{N_p}\right] \tag{6}$$

$$t = \left[\mathrm{t}_1, \mathrm{t}_2, \cdots, \mathrm{t}_{N_p}\right] \tag{7}$$

Step 3: For sampled data sequences of each mainlobe pulse signal, polynomial functions are adopted as basis functions, and the least square algorithm is utilized to complete the fitting of mainlobeenvelope curves.

The mainlobe envelope of the radar antenna exhibits inherent features of unimodal smooth variation, a single extreme value and steady bilateral attenuation, without irregular fluctuation components. First-order and second-order polynomials are only suitable for ideal symmetric mainlobesand cannot achieve a favorable fitting performance for asymmetric mainlobesunder beam deflection conditions. Fitting orders higher than five will amplify noise disturbance, arouse Runge oscillation, generate physically inconsistent fitting results and raise computational overhead, which cannot satisfy the requirement of real-time data processing. Therefore, the fitting order is restricted from 3 to 5, and an adaptive order selection strategy based on the sum of squared errors is established:

1. Extract valid amplitude sampling values within the coverage range of antenna mainlobe pulse sequences;
2. Perform least square fitting sequentially with polynomial orders of 3, 4 and 5. The general expression of a K-order polynomial is written as:

$$p(x) = p_1 x^K + p_2 x^{K-1} + p_3 x^{K-2} + \cdots + p_{K+1} \tag{8}$$

Define the sum of squared fitting errors as $p = \left[p_1, p_2, p_3, \cdots p_{K+1}\right]^T$, $J(p) = \sum_{\mathrm{k}=1}^{\mathrm{N_p}} \left[\widetilde{\mathrm{PA}_\mathrm{k}} - \mathrm{p}(\mathrm{t_k})\right]^2$. By setting the gradient of the error function equal to zero, namely, Let $\nabla J(p) = 0$, the standard normal equation can be derived as:

$$X^T X p = X^T y \tag{9}$$

where ∇ represents the differential operator. The design matrix and observation vector are constructed as follows:

$$X = \begin{bmatrix} t_1^K & t_1^{K-1} & & t_1 & 1 \\ \vdots & \vdots & \cdots & \vdots & \vdots \\ t_{N_p}^K & t_{N_p}^{K-1} & & t_{N_p} & 1 \end{bmatrix} \tag{10}$$

$$y = \left[\widetilde{PA}_1, \cdots \widetilde{PA}_{N_p}\right]^T \tag{11}$$

The optimal polynomial coefficient vector is solved by:

$$p = \left(X^T X\right)^{-1} X^T y \tag{12}$$

where $p = \left[p_1, p_2, p_3, \cdots p_{K+1}\right]^T$ denotes the undetermined coefficient vector of the fitted polynomial.

3. The sum of squared errors $J(p)$ is adopted as the quantitative index to evaluate fitting precision. A maximum allowable fitting error threshold S_0 is predefined for practical engineering applications. Under the constraint condition $J(p) \leq S_0$, the minimum feasible polynomial order is preferentially selected to comprehensively balance fitting accuracy and computational efficiency.

Step 4: Substitute the polynomial coefficients pi solved by the least square fitting and reconstruct the complete MBP curve combined with the time independent variable.

Step 5: Detect the vertex times $t_{i+1} = TOA(k_{i+1})$ and $t_i = TOA(k_i)$ of the MBP curves fitted from two adjacent groups of mainlobe pulses.

Step 6: Calculate the time difference $T = t_{i+1} - t_i$ between the vertices of two adjacent groups of main-lobe pulses, which is the radar antenna scan period.

3.2. Smoothing-Correlation Method

Drawing on the core idea of the radar pulse compression algorithm, this method selects a group of mainlobe pulses with stable amplitude peaks, no depression and high signal-to-noise ratio from the smoothed pulse sequence as the reference signal $s(n)$ for the cross-correlation operation. It performs cross-correlation between the reference signal $s(n)$ and the smoothed full-pulse amplitude sequence PA of the radar uses the peak characteristics of the cross-correlation function $R(k)$ to detect the time $t_i = TOA(k_i)$ corresponding to the peak position k_i and then calculates the scan period. Cross-correlation can effectively suppress random noise and significantly enhance the signal's periodic characteristics. Even under complex conditions such as amplitude distortion and fuzzy peak values, it can still identify the mainlobe position stably with strong anti-interference ability. The detailed implementation steps of the smoothing-correlation method are as follows:

Step 1: Same as the smoothing processing step of the smoothing-fitting method, the smoothed pulse amplitude sequence $\widetilde{PA}$.

Step 2: Construction and Dynamic Update of Mainlobe Reference Signal. From the smoothed pulse amplitude sequence, taking the total number of effective pulses of a single mainlobe as the benchmark, a continuous pulse segment accounting for 50~80% of the central interval is intercepted to construct the initial reference signal $s(n)$. The length of the reference signal is defined as M, and its selection rules are as follows:

1. M is set to an integer power of 2 to adapt to hardware-based fast correlation and FFT operations;
2. To ensure the stability of the reference signal, the constraint M $\geq$ 2L must be satisfied, where L denotes the moving average window length.

The number of effective pulses within the measured radar mainlobe in this paper is approximately 120. Intercepting according to the ratio of 50~80% yields a corresponding pulse interval length of 60~96. Under the constraints of being an integer power of 2 and no less than 2L (L = 30), the reference signal length is determined as M = 64.

The detailed implementation procedure for reference signal construction is given below:

1. In the smoothed mainlobe envelope, take the peak position as the center, and symmetrically intercept 64 consecutive points of pulse amplitude data to form a candidate reference signal.
2. Set an amplitude screening threshold. If the amplitude of any pulse in the candidate reference signal is lower than 60% of the mainlobe peak amplitude, it is determined that there is depression distortion, and the candidate reference signal is discarded.
3. Continuously store 10 frames of candidate reference signals that pass the screening and are free of obvious distortion.

4. After the storage queue is full, perform point-by-point arithmetic averaging on the 10 frames of qualified reference signals to generate the initial standard reference signal, and calculate the corresponding 64-point mainlobe width.
5. Introduce a dynamic update mechanism for the reference signal. In the subsequent streaming processing, judge the mainlobe width of each frame in real time. If the change in the mainlobewidth exceeds 10% compared with the initial standard reference signal, the reference signal will be re-constructed according to the above steps.

Step 3: Perform cross-correlation processing between the above reference signal s(n) and the complete smoothed radar full-pulse amplitude sequence to obtain the correlation output sequence:

$$R(k) = \sum_{n=0}^{M-1} \widetilde{PA}(k+n) \cdot s(n), \ \ k = 1, 2, \cdots, N - M \tag{13}$$

where $\widetilde{PA}(\cdot)$ denotes the smoothed pulse amplitude sequence, M is the length of the reference signal, and N is the length of the single-frame pulse sequence to be processed.

It is particularly worth noting that for conventional radar with uniform-speed mechanical circular scanning, the mainlobe scanning duration is much shorter than the antenna scanning period. Generally, the reference signal length M is no more than 1% of the single-frame pulse amplitude sequence to be processed. The computational complexity of time-domain sliding correlation is O(NM), which is much lower than O(N$\log_2$N) of frequency-domain correlation. Meanwhile, time-domain correlation does not require large-scale zero-padding for the reference signal sequence and avoids the aliasing problem caused by circular correlation. Furthermore, it supports point-by-point streaming sliding processing with low memory occupation and low processing latency. Therefore, the time-domain correlation method is superior to the frequency-domain counterpart in scenarios with short reference signal matching.

Step 4: Based on the peak characteristics of the cross-correlation function $R(k)$, the corresponding moments of adjacent valid peak positions are searched as $t_{i+1} = TOA(k_{i+1})$ and $t_i = TOA(k_i)$. The specific rules for peak searching are given as follows:

(1) Set an adaptive threshold for peak detection

According to the baseline mean μ and standard deviation σ of the sequence after correlation processing, an adaptive threshold T_h for the peak detection is calculated. Any peak lower than the threshold is directly judged as a false noise peak and eliminated.

(2) Set a peak width threshold

The main correlation peak corresponding to the real scanning period is generated by matching the complete mainlobe envelope and occupies a certain effective width. In contrast, false noise peaks mostly appear as narrow and isolated spikes with an effective width much smaller than that of real peaks. A minimum peak width threshold is predefined; any isolated spike narrower than this threshold is identified as a false peak.

(3) A priori constraint of peak interval

For radar systems with uniform-speed mechanical circular scanning, the physical range of the scanning period is known. The reasonable period interval of conventional mechanically scanned radars ranges from 2 s to 15 s. Candidate peaks with intervals falling within this physical range are regarded as real main peaks corresponding to the scanning period, while peaks with intervals shorter than 2 s or longer than 15 s are discarded.

Step 5: Calculate the time interval between adjacent peaks to finally obtain the radar antenna scan period $T = t_{i+1} - t_i$.

4. Verification with Measured Data

4.1. Verification of the Smoothing-Fitting Method

According to the implementation steps of the smoothing-fitting method described in Section 3.1, the window length of smoothing processing is first determined according to the jitter characteristics of the pulse amplitude value, and then the moving average smoothing processing is carried out on the original pulse amplitude data. To intuitively reflect the suppression effect of smoothing processing on noise and short-term amplitude fluctuation, three different smoothing window lengths of 10, 20 and 30 points are selected in this verification experiment to process the mainlobe pulse group composed of 10,000 pulse amplitudes.

Figures 4–7 show the comparison of the original four mainlobe pulse amplitude sequences with the smoothing effects of 10, 20 and 30 points in turn. The experimental results show that the larger the smoothing window length, the more significant the suppression effect on pulse amplitude jitter and the smaller the curve fluctuation. It can be seen from Figures 4–7 that there is significant instability in the maximum pulse value. If the peak is directly detected by using the single-point maximum value, accurate peak points cannot be obtained, which is likely to introduce large measurement errors. Therefore, replacing the single-point peak value with the overall characteristics of the mainlobe envelope can suppress the estimation deviation caused by the instability of the maximum value, thereby ensuring the measurement accuracy and robustness of the antenna scanning period. Figure 8 shows the fitting approximation effect of each group of mainlobe pulse sequences by the least square method after 30-point smoothing. The results show that the fitted MBP curve effectively eliminates the adverse interferences, such as depression and flat segments in the original mainlobe pulse amplitude, and all curves present regular convex peak characteristics. On this basis, the peak search algorithm can be used to accurately locate the time corresponding to the vertex of each group of mainlobe pulse sequences.

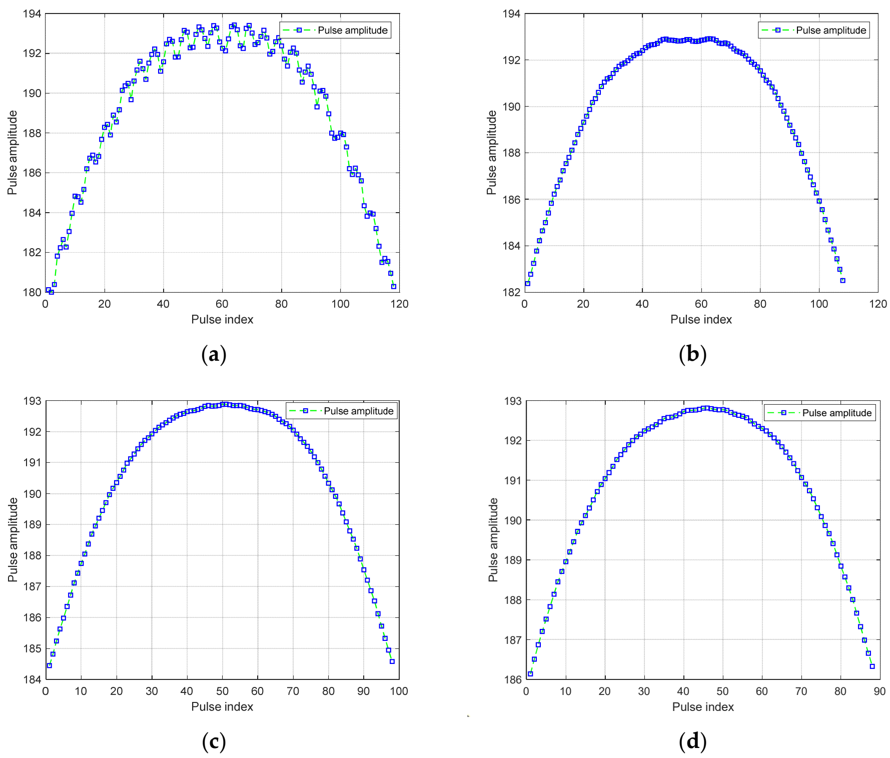

Figure 4. Comparison of smoothing effects with different points for the first mainlobe pulse amplitude sequence: (**a**) Filed-measured mainlobe pulse amplitude sequence; (**b**) 10-point smoothing result; (**c**) 20-point smoothing result; (**d**) 30-point smoothing result.

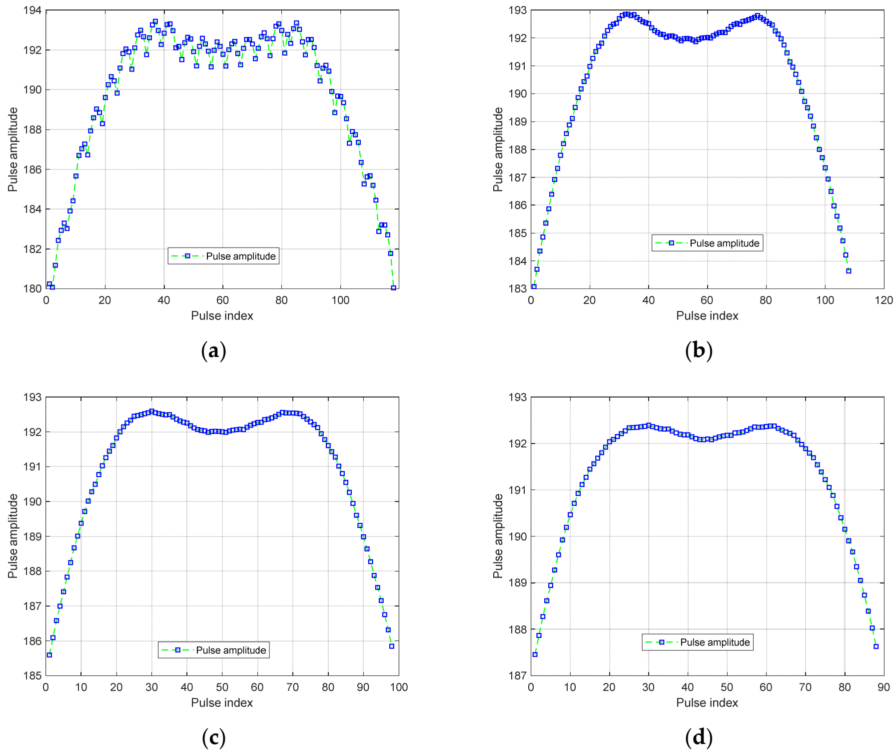

Figure 5. Comparison of smoothing effects with different points for the second mainlobe pulse amplitude sequence: (**a**) Filed-measured mainlobe pulse amplitude sequence; (**b**) 10-point smoothing result; (**c**) 20-point smoothing result; (**d**) 30-point smoothing result.

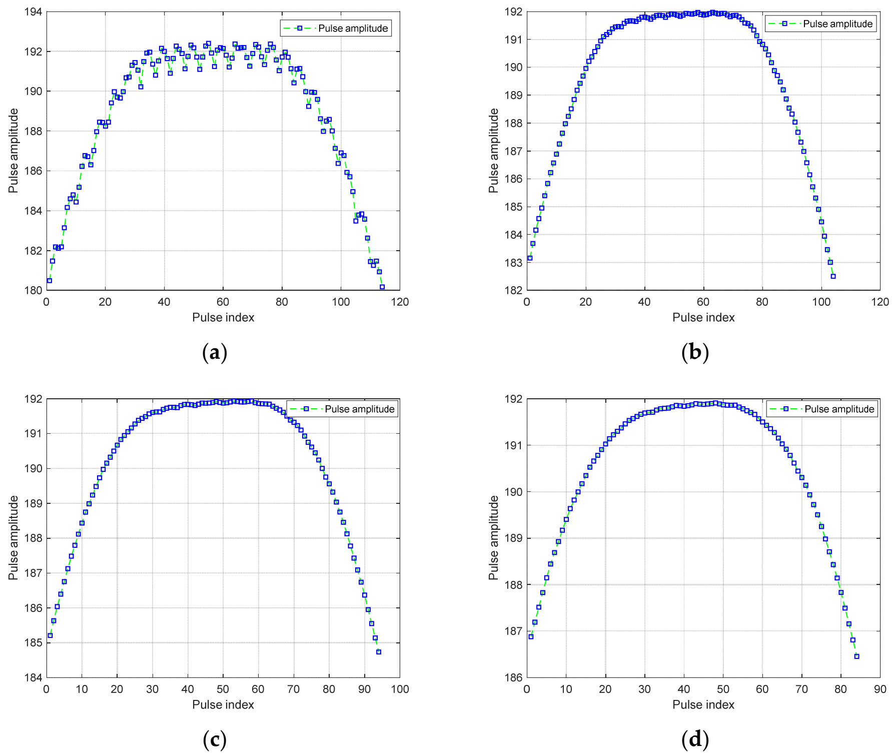

Figure 6. Comparison of smoothing effects with different points for the third mainlobe pulse amplitude sequence: (**a**) Filed-measured mainlobe pulse amplitude sequence; (**b**) 10-point smoothing result; (**c**) 20-point smoothing result; (**d**) 30-point smoothing result.

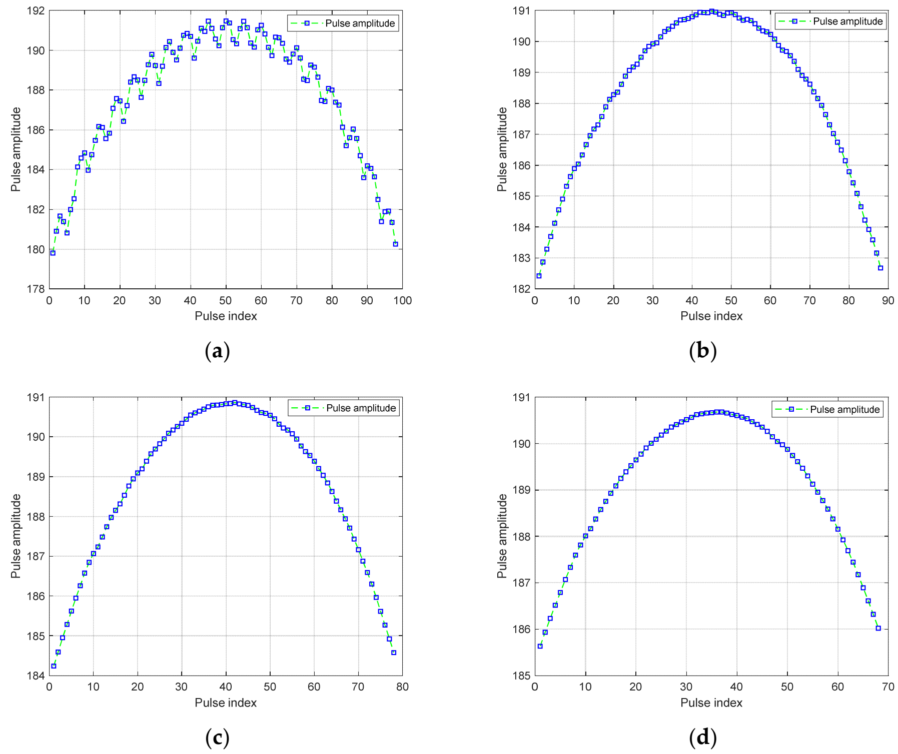

Figure 7. Comparison of smoothing effects with different points for the fourth mainlobe pulse amplitude sequence: (**a**) Filed-measured mainlobe pulse amplitude sequence; (**b**) 10-point smoothing result; (**c**) 20-point smoothing result; (**d**) 30-point smoothing result.

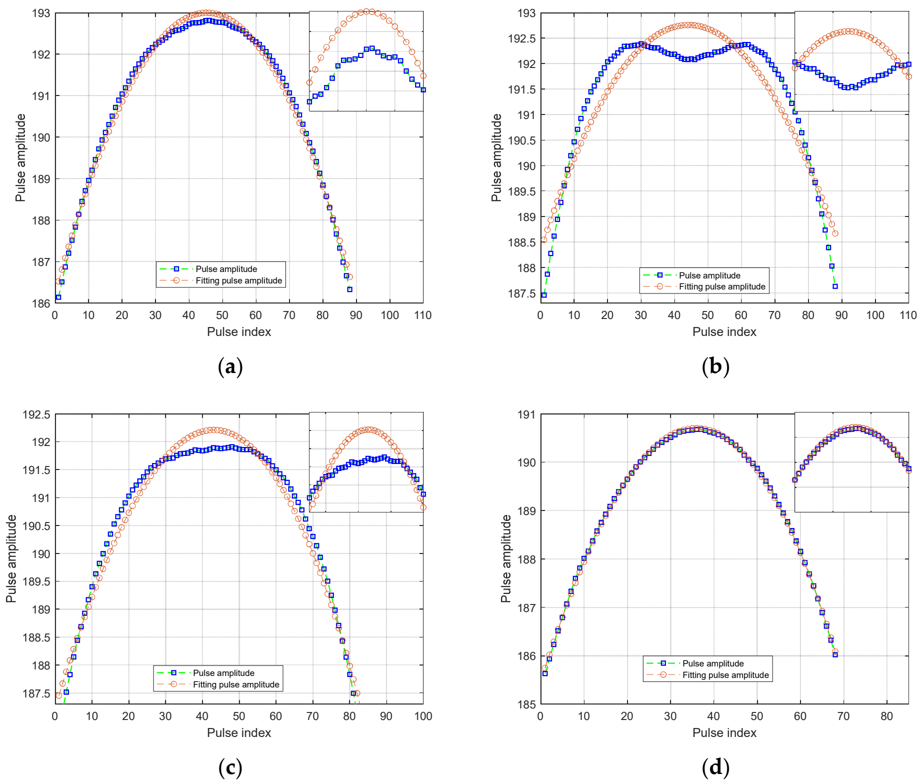

Figure 8. Comparison of least square fitting effects for four mainlobe pulse amplitude sequences (blue dots: amplitude values of pulse sequences after 30-point smoothing; orange dots: least square fitting MBP curves): (**a**) The first MBP curve; (**b**) The second MBP curve; (**c**) The third MBP curve; (**d**) The fourth MBP curve.

Table 1 shows the complete results of the radar scan period measurement for 10,000 pulse sequences based on the smoothing-fitting method. After measurement, the number of pulses ΔN between the vertices of four adjacent mainlobes is 2720, 2722 and 2720 in turn, with $\Delta N \in [2720, 2722]$ and the error jitter $\leq$ 2 PRIs. Converted with the pulse repetition interval of 3.65 ms, the measured values of the antenna scan period are 9.928 s, 9.935 s and 9.928 s, respectively. Comparing the measured values with the nominal radar antenna scan period of 10 s, the relative measurement error is 0.72%, which meets the requirements of engineering applications.In the statistical results of the fitting error at the vertex time in Table 1, only two outlier samples with relatively large errors appear in the third group of mainlobe pulse sequences. Through retrospective analysis of the original pulse waveform, it is found that this anomaly is caused by the excessively flat waveform at the peak of the mainlobe, blunted peak characteristics, consistent amplitude in the top interval, and the lack of a significant and unique extreme point. During the envelope fitting and vertex optimization process, the flat-top effect reduces the uniqueness of peak position identification, thereby introducing a small deviation in the time estimation.

Table 1. Measurement results of the smoothing-fitting method.

Index	First Mainlobe Vertex	Second Mainlobe Vertex	Third Mainlobe Vertex	Fourth Mainlobe Vertex
Numbercorresponding to the mainlobe peak	1026	3746	6468	9188
Pulse count between mainlobe peak points	-	2720	2722	2720
Antenna scan period (s)	-	9.928	9.935	9.928

4.2. Verification of the Smoothing-Correlation Method

According to the implementation steps of the smoothing-correlation method in Section 3.2, the number of smoothing processing data points is determined according to the pulse amplitude jitter characteristics. To ensure the consistency of experimental conditions with the smoothing-fitting method for subsequent comparative analysis, the number of smoothing data points selected by the smoothing-correlation method is the same as that of the smoothing-fitting method, both set to 30. Figure 9 shows the processing effect of 30-point smoothing on 10,000 pulse amplitude sequences, and Figure 10 shows the 30-point smoothed pulse amplitude sequences of the four radar mainlobes.

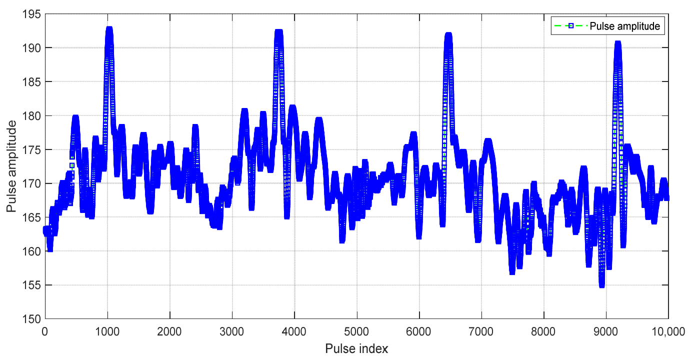

Figure 9. Radar mainlobe pulse amplitude sequence after 30-point smoothing processing.

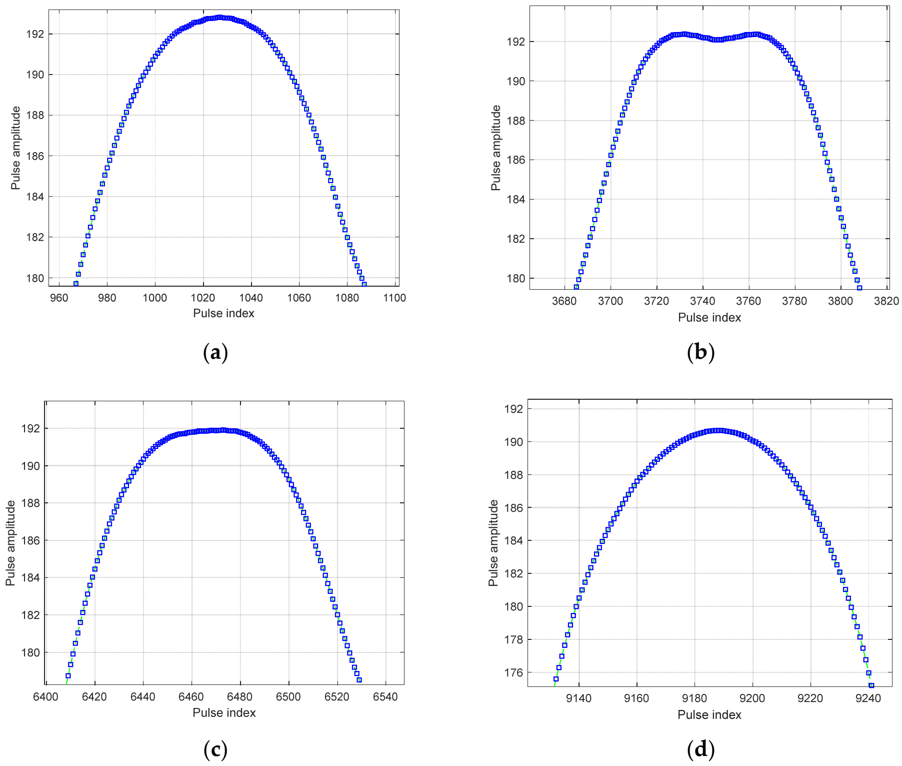

Figure 10. Comparison of smoothing effects for four mainlobe pulse amplitude sequences: (**a**) The first mainlobe pulse amplitude sequence; (**b**) The second mainlobe pulse amplitude sequence; (**c**) The third mainlobe pulse amplitude sequence; (**d**) The fourth mainlobe pulse amplitude sequence.

The first mainlobe pulse amplitude sequence is selected as the sample signal to perform a cross-correlation operation with the 30-point smoothed 10,000 pulse amplitude sequences, and the operation results are shown in Figure 11. Figure 12 shows the four radar mainlobe pulse amplitude sequences after correlation processing. Comparing Figure 12b with Figure 10b, the amplitude depression problem in the mainlobe pulse amplitude sequence is effectively eliminated after correlation processing; comparing Figure 12c with Figure 10c, the waveform of the mainlobe pulse sequence is more prominent after processing, which completely solves the defect of excessively flat original mainlobe pulse amplitude. Then the peak search algorithm is used to locate the time corresponding to the vertex of each mainlobe pulse sequence.

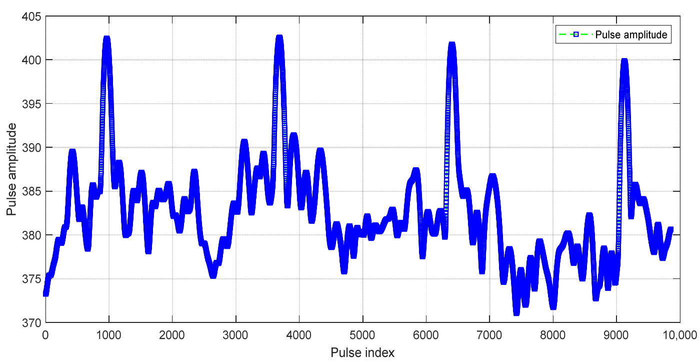

Figure 11. Pulse amplitude sequence after correlation processing.

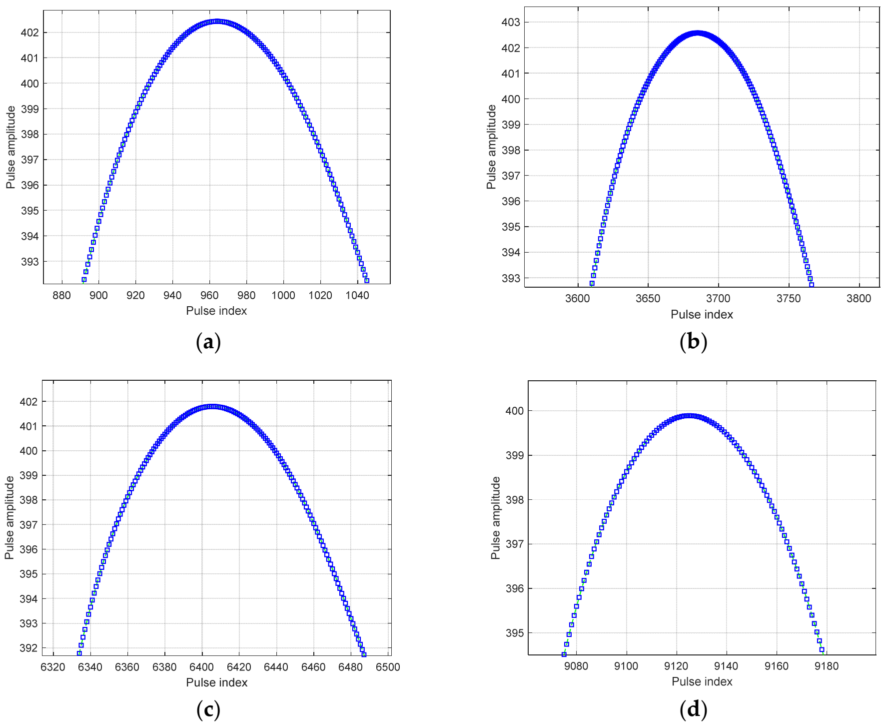

Figure 12. Comparison of smoothing-correlation processing effects for four mainlobe pulse amplitude sequences: (**a**) The first mainlobe pulse amplitude sequence; (**b**) The second mainlobe pulse amplitude sequence; (**c**) The third mainlobe pulse amplitude sequence; (**d**) The fourth mainlobe pulse amplitude sequence.

Table 2 lists the final results of the radar scan period measurement for 10,000 pulse sequences by the smoothing-correlation method. After detection, the number of pulses ΔN between the vertices of four adjacent mainlobes is 2721, 2720 and 2720 in turn, with $\Delta \mathrm{N} \in [2720, 2721]$, and the error jitter is no more than 1 PRI. Calculated with the PRI of 3.65 ms, the measured antenna scan periods are 9.932 s, 9.928 s and 9.928 s, respectively. Comparing the measured values with the nominal radar antenna scan period of 10 s, the relative measurement error is 0.72%, which meets the requirements of engineering applications.

Table 2. Measurement results of the smoothing-correlation method.

Index	First Mainlobe Vertex	Second Mainlobe Vertex	Third Mainlobe Vertex	Fourth Mainlobe Vertex
Numbercorresponding to the mainlobe peak	964	3685	6405	9125
Pulse count between mainlobe peak points	-	2721	2720	2720
Antenna scan period (s)	-	9.932	9.928	9.928

4.3. Comparative Experiment with Traditional Measurement Methods

To verify the comprehensive performance of the smoothing-fitting method and smoothing-correlation method proposed in this paper, three classic radar antenna scan period measurement methods are selected as the control group to carry out a multi-dimensional quantitative comparative experiment. The experiment adopts the same set of filed-measured PDW data (a total of 10,000 pulse data with a total duration of 36 s). Five core indicators, including error fluctuation, relative error, number of floating-point calculations, number of cache points and streaming processing adaptability, are selected from three dimensions of measurement accuracy, calculation efficiency, and engineering implementation adaptability to evaluate the advantages and disadvantages of each method, providing a reliable basis for engineering application selection.

4.3.1. Comparison Methods and Experimental Conditions

The three classic radar antenna scan period measurement methods selected in this experiment are the traditional threshold method, curve fitting method and spectrum estimation method, which are compared with the two methods proposed in this paper. The principles and implementation modes of various methods are as follows:

(1) Traditional control methods

Traditional threshold method [6]: Traverse the amplitude sequence with length N, compare each point with the threshold, record the start index n_s and end index n_e of the mainlobe, calculate the mainlobe center position as $n_c = (n_s + n_e)/2$, obtain the interval between two adjacent mainlobes as $\Delta n = n_{c2} - n_{c1}$, and convert it to the scan period $\mathrm{T} = Toa_{n_{c2}} - Toa_{n_{c1}}$. This method does not require complex operations and has a fast calculation speed, but it is extremely susceptible to noise interference, signal amplitude depression, flat amplitude and other factors with poor robustness.

Curve fitting method [12]: Traverse the amplitude sequence with length N, compare each point with the threshold, record the start index n_s and end index n_e of the mainlobe, adopt polynomial fitting to the pulse amplitude sequence between n_s and n_e to reconstruct the antenna mainlobe curve, then locate the peak point of the antenna mainlobe curve through the peak search algorithm, and calculate the scan period according to the peak interval of adjacent mainlobe curves. Compared with the threshold method, this method has improved accuracy, but the fitting process relies on batch-complete data, is sensitive to noise, and cannot adapt to real-time streaming data processing.

Spectrum estimation method [15]: Obtain the scanning modulation frequency by performing FFT on the amplitude sequence with length N, find the spectral peak position k_{peak} corresponding to the antenna scan period, with the corresponding frequency $f = k_{peak} \times f_s/N$, and infer the time-domain scan period $\mathrm{T} = \mathrm{N}/\left(k_{peak} \times f_s\right)$. This method is suitable for stationary signal measurement; when facing non-stationary filed-measured data with sudden interference, the spectrum is prone to false peaks leading to measurement failure, and it has a large amount of computation and poor real-time performance.

(2) Methods proposed in this paper

The smoothing-fitting method and smoothing-correlation method adopt 30-point sliding window smoothing preprocessing to first suppress noise and short-term amplitude fluctuation and then realize high-precision extraction of the scan period through fitting optimization and cross-correlation operation, respectively. The specific steps are the same as those described above.

(3) Experimental environment

All methods in this paper are carried out on the same filed-measured dataset, with the same mainlobe extraction interval and a unified computing platform. The hardware and software environment used are Dell Precision 7865 Tower (Dell Technologies Inc., Round Rock, TX, USA) and Matlab R2021a (The MathWorks, Inc., Natick, MA, USA). In the experiment, the mainlobe judgment interval, data interception length and peak optimization threshold are unified, and all methods are measured 100 times repeatedly, with the average value taken as the final result to reduce random errors.

4.3.2. Performance Comparison Results

Let the length of the pulse amplitude sequence be N (N = 10,000), the number of mainlobes be P (P = 4), the sliding window length be L (L = 30), the reference signal length be M (M = 64), the order of polynomial fitting be K (K = 3), and the number of fitted mainlobe pulses be N_p(N_p = 100). Through experimental testing, the comparison results of the five measurement methods on the five core indicators are obtained, with all indicators taking the average value of multiple experiments, and the data is stable and reliable, as shown in Table 3 in detail.

Table 3. Performance comparison of radar antenna scan period measurement methods.

Measurement Method	Error Fluctuation (Number of PRI)	Max Relative Error (%)	Number of Floating-Point Calculations	Number of Cache Points	Stream Processing Adaptability
Traditional threshold method	13	6.2	$3(P-1)$	0	High
Curve fitting method	4	3.5	$10N_p + 33$	N_p	Low
Spectrum estimation method	7	6.1	$N\log_2 N + 5N$	N	Medium
Smoothing-fitting method	2	1.3	$LN + 10N_p + 33$	$L + N_p$	Low
Smoothing-correlation method	1	0.9	$LN + (N-M+1)(2M-1) + 1$	L	High

Note: Error fluctuation is in pulse repetition intervals, with smaller values indicating higher measurement stability; relative error is the percentage deviation between the measured value and the nominal value, with smaller values indicating higher accuracy; the number of floating-point calculations reflects the computational efficiency of the method, with fewer calculations indicating better real-time performance; the number of cache points and streaming processing adaptability reflect whether the method can adapt to real-time pulse stream processing, which determines the difficulty of engineering implementation.

4.3.3. Performance Comparison Analysis

Combined with the data in Table 3, an in-depth analysis of the five measurement methods is carried out from three core dimensions of measurement accuracy, processing efficiency and engineering adaptability to evaluate the applicable scenarios, advantages and disadvantages of each method.

1. Comparison of measurement accuracy

The traditional threshold method judges the mainlobe by a fixed amplitude threshold without any anti-interference measures, and is extremely significantly affected by outdoor noise, signal amplitude depression, flat amplitude and other factors, with an error fluctuation of up to 13 PRIs and a relative error of 6.2%. The measurement results fluctuate greatly with extremely low accuracy, which cannot meet the engineering requirements, and are only suitable for the ideal environment with no interference and excellent signal quality. Compared with the threshold method, traditional optimization methods, such as the curve fitting method and spectrum estimation method, have improved accuracy, with the error fluctuation reduced to 4 PRIs and 7 PRIs, and the relative error of 3.5% and 6.1%, respectively. However, there are still large deviations, and when facing complex filed-measured data, they are prone to fitting distortion and spectral false peak interference, with insufficient measurement stability.

The two methods proposed in this paper filter out noise and short-term random fluctuations in advance through sliding window smoothing preprocessing, which greatly reduces the impact of interference and achieves a qualitative improvement in measurement accuracy. Among them, the error fluctuation of the smoothing-fitting method is controlled within 2 PRIs with a relative error of only 1.3%; the smoothing-correlation method has better accuracy, with the error fluctuation no more than 1 PRI and a relative error as low as 0.9%, which is far superior to traditional methods and fully meets the engineering requirements for high-precision measurement.

It can be concluded from the comparison of three core engineering dimensions, including computational complexity, processing latency and noise robustness, that the smoothing-fitting method is affected by the actual number of sampling points of the mainlobe, resulting in fluctuating computational workload. It requires caching complete mainlobe data for batch fitting, which leads to high processing latency and high sensitivity to noise, pulse loss and waveform distortion. By contrast, the smoothing-correlation method adopts a fixed-length reference template with constant and controllable computational complexity. It achieves low-latency real-time processing relying on the point-by-point sliding mechanism and possesses stronger anti-interference capability by virtue of coherent accumulation characteristics, thus delivering better engineering adaptability and practical deployment potential. A comprehensive comparison of the engineering performance of the two methods is presented in Table 4.

Table 4. Comprehensive comparison of engineering performance between the two methods.

Evaluation Index	The Smoothing-Fitting Method	The Smoothing-Correlation Smoothing-Correlation
Computational complexity	O(NL + KNp)	O(NL + NM)
Processing Latency	high	low
Robustness to noise	Moderate	Strong

2. Comparison of processing efficiency

The traditional threshold method has an extremely simple operation logic, only requiring threshold judgment and a small amount of subtraction, with the number of floating-point calculations of only $3(P - 1)$. It has the smallest amount of computation and extremely high real-time performance with almost no computational overhead, but at the cost of measurement accuracy, belonging to a low-cost and low-precision measurement method. The curve fitting method needs to complete two core operations of batch data fitting and peak search, with a computational amount of $10N_p + 33$, a small amount of computation and good real-time performance, performing limited fitting operations only in the mainlobe interval; the spectrum estimation method needs to perform complex operations such as the Fourier transform and spectral peak search, with a computational amount of $N\log2N + 5N$, whose computational overhead is significantly higher than that of the time-domain method with poor real-time performance.

Different from the smoothing-fitting method, which performs fitting on a complete single mainlobe envelope, the smoothing-correlation method conducts point-by-point sliding matching between a fixed mainlobe reference template and streaming pulse amplitude sequences, achieving superior robustness under complex conditions such as low signal-to-noise ratio, pulse missing, and multipath interference. In terms of resource consumption, the smoothing-fitting method only needs to cache the current complete mainlobe data for fitting and does not require long-term streaming buffering. In comparison, the smoothing-correlation method needs to store the fixed reference template and maintain sliding data buffers, leading to a slight increase in memory usage and computational complexity. Nevertheless, the template length is only 64 points, and the additional resource overhead is limited and acceptable in practical engineering applications. This method realizes a noticeable improvement in streaming processing accuracy and anti-interference performance at the cost of a slight increment in memory and computational resources.

However, it is still within the bearable range of embedded hardware and can meet the requirements of engineering real-time processing. For example, in a typical engineering parameter scenario, the length of a single-frame pulse amplitude sequence is $N = 10{,}000$, the reference template length is $M = 64$, and the smoothing window length is $L = 30$. Substituting into the formula $LN + (N - M + 1)(2M - 1) + 1$, the total number of single-frame floating-point operations of the smoothing-correlation method is approximately 1.562 million. Using the TMS320C6678 DSP (Texas Instruments Incorporated, Dallas, TX, USA) as the hardware carrier, estimated with the single-core theoretical floating-point peak computing power of 20 GFLOPS, the theoretical processing time of a single frame of the algorithm is about 78.1 μs. Even considering the performance loss caused by the actual DSP operating efficiency (usually 30% to 60% of the theoretical peak), instruction scheduling, memory access, and data interaction in engineering practice, the actual processing time is still much less than the antenna scanning period constraint of 2 s to 15 s for conventional mechanically scanned radars, with sufficient real-time margin. Therefore, the proposed algorithm has strong engineering feasibility on the existing embedded signal processing platform and can meet the application requirements of pipeline real-time processing.

3. Comparison of engineering adaptability

The traditional threshold method has 0 cache points, no need to store historical data, high streaming processing adaptability, extremely low resource occupation, and is very easy to deploy on embedded platforms. The curve fitting method needs to cache N_p pulse data cannot output results in a point-by-point streaming manner, has low adaptability, and is suitable for offline or non-strict real-time scenarios. The spectrum estimation method needs to cache the full-segment N-point data, relies on full-segment FFT, only supports moderate streaming processing, has large resource occupation and high storage requirements.

Among the two methods in this paper, the smoothing-fitting method only needs to cache a sliding window with length L, with small storage overhead, but has low streaming adaptability due to relying on post-fitting output. The smoothing-correlation method needs to cache the window L and the reference signal M, with a total cache of L + M and small storage overhead. In addition, it adopts the logic of point-by-point sliding and real-time operation, which is fully compatible with streaming pulse data processing. Its processing flow is highly consistent with the existing pulse compression algorithm flow, without modifying the original hardware architecture and software flow, with extremely low deployment difficulty and strong engineering implementation capability.

4. Comprehensive Conclusion

Based on the above comparative analysis from three dimensions, the applicable scenarios and comprehensive performance of the five radar antenna scan period measurement methods are significantly different: the core advantages of the traditional threshold method are simple calculation, no cache requirement, high streaming adaptability and extremely low resource occupation, but its measurement accuracy is extremely poor and anti-noise ability is weak, only suitable for scenarios with extremely low requirements for measurement accuracy and extremely limited hardware resources. The curve fitting method achieves a certain compromise between measurement accuracy and processing efficiency, with higher accuracy than the traditional threshold method and controllable computation amount, but poor engineering adaptability and no support for streaming processing, suitable for offline processing scenarios with low real-time requirements and the pursuit of medium measurement accuracy. The spectrum estimation method has poor comprehensive performance, with no obvious advantages in measurement accuracy, and at the same time has a large amount of computation and storage overhead, with medium engineering adaptability. Under the test conditions of this paper, it has no obvious competitiveness compared with other methods and has limited applicable scenarios. The smoothing-fitting method has high measurement accuracy, moderate computation amount and small storage demand, which can achieve a good balance between accuracy and computational overhead, suitable for application scenarios with high requirements for measurement accuracy and certain acceptable computational overhead. The smoothing-correlation method achieves the optimal comprehensive performance, with its measurement accuracy being significantly leading among the five methods. It is consistent with the existing pulse compression algorithm processing architecture and has high engineering adaptability and low storage overhead. Although it has the largest amount of computation, it can be accelerated by FFT,

https://doi.org/10.3390/electronics15112249

which significantly improves real-time performance, making it the preferred solution for high-precision radar antenna scan period measurement scenarios.

5. Conclusions

Aiming at the filed-measured radar full-pulse data, which exhibits the characteristics of pulse amplitude jitter, distortion and loss caused by multiple non-ideal factors such as slight movement (static platform) or even motion (airborne platform) of the radar platform, signal propagation attenuation, complex electromagnetic interference and equipment measurement errors, this paper adopts sliding window smoothing processing to suppress noise and short-term random fluctuations, and proposes two high-precision measurement methods for the radar antenna scan period: the smoothing-fitting method and the smoothing-correlation method, and gives the complete implementation flow. Verification with filed-measured data shows that the error fluctuation of the antenna period measured by the smoothing-fitting method is controlled within 2 PRIs, and that measured by the smoothing-correlation method is controlled within 1 PRI, both meeting the accuracy requirements of engineering applications. Compared with the traditional threshold method, curve fitting method and spectrum estimation method, the smoothing-fitting method and smoothing-correlation method have smaller error fluctuation and higher computational efficiency. Compared with the smoothing-fitting method that requires a data fitting operation, the smoothing-correlation method has a processing flow more suitable for streaming data processing, which is consistent with the existing pulse compression algorithm processing architecture. It possesses mature conditions for practical engineering deployment and can be directly embedded and integrated into existing radar reconnaissance signal processing systems for field application.

This study still has clear applicable boundaries and limitations. The proposed methods are mainly designed for the mechanical uniform-speed circular scanning mode and are suitable for conventional detection scenarios with a constant scanning period and stable pulse amplitude envelope morphology. For the time-varying scanning period and dynamic envelope distortion caused by complex working conditions, such as the complex adaptive scanning mode of phased array radar, the fitting and correlation matching strategies are difficult to be directly applied. Facing the above limitations, future research can be further carried out on the high-precision measurement technology of the antenna scanning period for the complex adaptive scanning of phased array radar.

Author Contributions: Data curation, investigation, writing—original draft preparation, Formal analysis, B.W.; Funding acquisition, Project administration, Resources, Supervision, Writing—review and editing, M.W.; Conceptualization, Methodology, Software, Visualization, B.W. and M.W. All authors have read and agreed to the published version of the manuscript.

Funding: This research was funded by the National Natural Science Foundation of China (Grant Nos. 61420106011 and 61572307).

Data Availability Statement: The data that support the findings of this study are available from the corresponding author upon reasonable request.

Conflicts of Interest: The authors declare no conflicts of interest.

Abbreviations

The following abbreviations are used in this manuscript:

PDW	Pulse Description Word
PA	Pulse Amplitude
TOA	Time of Arrival
RF	Radio Frequency

DOA	Direction of Arrival
PRI	Pulse Repetition Interval
MBP	Mainlobe Pattern
FFT	Fast Fourier Transform

References

1. Adamy, D. *EW 101: A First Course in Electronic Warfare*, 4th ed.; Artech House: Norwood, MA, USA, 2015; pp. 7–8.
2. Skolnik, M.I. *Radar Handbook*, 3rd ed.; McGraw-Hill Education: New York, NY, USA, 2008; pp. 35–36.
3. Skolnik, M.I. *Introduction to Radar Systems*, 3rd ed.; McGraw-Hill: New York, NY, USA, 2002; pp. 46–49.
4. Adamy, D. *EW 102: A Second Course in Electronic Warfare*; Artech House: Norwood, MA, USA, 2003; pp. 67–68.
5. Adamy, D. *EW 104: EW Against A New Generation of Threats*; Artech House: Norwood, MA, USA, 2015; pp. 54–56.
6. Kang, Z.; Li, X.; Zhang, F. Study on accurately measuring technology about radar antenna scanning cycle. *Aerosp. Electron. Warf.* **2015**, *31*, 62–64.
7. Liu, S.; Lei, Z.; Ge, Y.; Wen, Z. Automatic radar antenna scan type recognition based on limited penetrable visibility graph. *J. Syst. Eng. Electron.* **2021**, *32*, 437–446. [CrossRef]
8. Wang, J.; Fang, M.; Zhang, W.; Wang, G.; Chen, Y.; Wu, P. Radar Antenna Scan Period Measurement Method, Device, Equipmentand Storage Medium. Chinese Patent CN111371436A, 3 July 2020.
9. Wang, B.; Wang, S.; Wang, J. Convolutional neural network-based radar antenna scanning period recognition. *Electronics* **2022**, *11*, 1383. [CrossRef]
10. Wang, B.; Wang, H.; Wang, S.; Wang, Y.; Zeng, D.; Wang, M. Recognition of the Radar Antenna Scanning Period based on Convolutional Neural Network. In *Proceedings of the 2019 IEEE International Conference on Signal, Information and Data Processing (ICSIDP), Chongqing, China, 11–13 December 2019*; IEEE: New York, NY, USA, 2019. [CrossRef]
11. Kalfaoglu, M.E.; Can, O.; Yildirim, B.; Alatan, A.A. Antenna scan period estimation of radars with cepstrum and scoring. In *Proceedings of the 2019 27th Signal Processing and Communications Applications Conference (SIU), Sivas, Türkiye, 24–26 April 2019*; IEEE: New York, NY, USA, 2019; pp. 1–4. [CrossRef]
12. Wan, P.; Hao, B.; Li, Z.; Ma, X.; Zhao, Y. Accurate estimation the scanning cycle of the reconnaissance radar based on a single unmanned aerial vehicle. *IEEE Access* **2017**, *5*, 22681–22689. [CrossRef]
13. Ma, X.; Zhang, H.; Hao, B.; Wan, P. Antagonistic estimation method of reconnaissance radar antenna scan period. *J. Xidian Univ.* **2018**, *45*, 161–165.
14. Huang, Z. Measurement method of antenna scan period based on discrete Fourier transform. *Shipboard Electron. Countermeas.* **2021**, *44*, 57–60.
15. Huang, Z.; Tang, B.; Qin, L. A fast estimation method for radar antenna scan period. *Electron. Inf. Warf. Technol.* **2024**, *39*, 31–35.